Incorporation of Pure Fullerene into Organoclays

Tsoufis, Theodoros; Georgakilas, Vasileios; Ke, Xiaoxing; Van Tendeloo, Gustaaf; Rudolf, Petra; Gournis, Dimitrios

Published in:
Chemistry

DOI:
10.1002/chem.201300164

DOI: 10.1002/chem.201300164

Incorporation of Pure Fullerene into Organoclays: Towards C_{60}-Pillared Clay Structures

Theodoros Tsoufis,*[a] Vasileios Georgakilas,[b] Xiaoxing Ke,[c] Gustaaf Van Tendeloo,[c] Petra Rudolf,[a] and Dimitrios Gournis[d]

Abstract: In this work, we demonstrate the successful incorporation of pure fullerene from solution into two-dimensional layered aluminosilicate minerals. Pure fullerenes are insoluble in water and neutral in terms of charge, hence they cannot be introduced into the clay galleries by ion exchange or intercalation from water solution. To overcome this bottleneck, we organically modified the clay with quaternary amines by using well-established reactions in clay science in order to expand the interlayer space and render the galleries organophilic. During the reaction with the fullerene solution, the organic solvent could enter into the clay galleries, thus transferring along the fullerene molecules. Furthermore, we demonstrate that the surfactant molecules, can be selectively removed by either simple ion-exchange reaction (e.g., interaction with $Al(NO_3)_3$ solution to replace the surfactant molecules with Al^{3+} ions) or thermal treatment (heating at 350 °C) to obtain novel fullerene-pillared clay structures exhibiting enhanced surface area. The synthesized hybrid materials were characterized in detail by a combination of experimental techniques including powder X-ray diffraction, transmission electron microscopy, X-ray photoemission, and UV/Vis spectroscopy as well as thermal analysis and nitrogen adsorption–desorption measurements. The reported fullerene-pillared clay structures constitute a new hybrid system with very promising potential for the use in areas such as gas storage and/or gas separation due to their high surface area.

Keywords: clays · fullerenes · hybrids · organoclays · pillared clays

Introduction

Buckminsterfullerene (C_{60}) with its perfect icosahedral symmetry still remains deeply fascinating as a building block for the construction of complex architectures. Fullerenes have been extensively studied during the past two decades,[1] especially after the development of methods to overcome one of their major drawback, namely the limited solubility of these all-carbon cages in polar solvents, and their consequent incorporation into various solid matrices (such as polymers[2] and glasses[3]) as well as porous materials (such as layered double hydroxides[4] and molecular sieves[5]).

In recent years, one-, two-, and three-dimensional assemblies where order and organization follow supramolecular principles, have assumed remarkable importance.[6] The challenge to be achieved is to control the organization of the assemblies and therefore their physical and chemical properties, through simple external parameters or variables, with the intent of creating new tailored materials. Among the tools exploitable for the creation of new assemblies are hydrophilic and hydrophobic forces. In addition to the magnitude of the forces, the formation of one particular spatial arrangement over another is also governed by the geometrical features of the chosen building blocks.

Smectite clays are a class of layered aluminosilicate minerals with a unique combination of swelling, intercalation, and ion-exchange properties that make these nanostructures valuable in diverse fields.[7] They consist of an octahedral alumina layer fused between two tetrahedral silica layers to constitute 9.6 Å thick platelets, which stack on top of each other separated by galleries. The cation-exchange capacity of a particular clay depends on the substitution of low-valence ions, for example, Mg^{2+} for Al^{3+} in the octahedral sheet and Al^{3+} for Si^{4+} in the tetrahedral sites. As a consequence, each layer has a fixed negative charge and neutrality is obtained for example, by hydrated cations present in the galleries between the sheets. The intercalation process in these systems is equivalent to an ion exchange, and unlike for intercalation compounds of graphite, it does not necessarily involve charge transfer between the guest and host species. The charge on the platelets affects many fundamental

[a] Dr. T. Tsoufis, Prof. Dr. P. Rudolf
Zernike Institute for Advanced Materials
University of Groningen, Nijenborgh 4
9747 AG Groningen (Netherlands)
E-mail: theodoros.tsoufis@gmail.com

[b] Prof. Dr. V. Georgakilas
Department of Materials Science
University of Patras, 26504 Rio (Greece)

[c] Dr. X. Ke, Prof. Dr. G. Van Tendeloo
EMAT, University of Antwerp
Groenenborgerlaan 171, 2020 Antwerp (Belgium)

[d] Prof. Dr. D. Gournis
Department of Materials Science & Engineering
University of Ioannina, 45110 Ioannina (Greece)

Supporting information for this article is available on the WWW under http://dx.doi.org/10.1002/chem.201300164.

properties of the clays, including cation fixation, swelling ability, water sorption, and the available specific surface area. These materials have the natural ability to adsorb organic or inorganic cationic guest species (and even neutral molecules) from solutions, and it is this cation "storage" that renders clay minerals uniquely suitable as catalysts,[8] templates[9] for the immobilization of molecules, or as components for composite materials.[10] The nature of the microenvironment between the aluminosilicate platelets regulates the topology of the intercalated molecules and affects possible supramolecular rearrangements or reactions, such as self-assembly processes that are usually not easily controlled in solution.[11]

Pillared clays are microporous solids formed by the intercalation of robust cations in the galleries (interlayers) of the smectite clays and similar 2:1-layered silicate-type structures.[7a] By adjusting the size of the pillaring cations and the separation between them, one can vary the pore size distribution over a broad range and thereby design micro- and nanoporous environments different from those afforded by conventional three-dimensional materials for example, zeolites. Thus, pillared clays provide a tunable intra-crystalline space valuable for shape-selective adsorption and catalysis.[12]

Recently, we described the intercalation of positively charged fulleropyrrolidine monoadduct[13] and a bisadduct[14] derivatives into aluninosilicate minerals through ion-exchange reactions and studied the effect of spatial confinement on the properties of these molecules. We found that a sizable amount of charge transfer takes place between the host and the guests but that not all the clay galleries were filled with the fullerene derivatives—probably due to the low solubility of the guest molecules. The type of the host clay strongly influenced the chemical form, the amount, and the conformation of the guest molecule in the cases where the C_{60} chemical derivatives were inserted into the galleries of the phyllomorphous materials. However, in all cases covalent chemical functionalization of fullerene was necessary in order to achieve partial or full solubility in water and thus ion-exchange-driven intercalation into the clay. This covalent chemical functionalization breaks the perfect icosahedral symmetry of C_{60}, thereby strongly influencing its properties.[15] In addition, this complicated, environmental unfriendly and costly chemical functionalization is restricting for up-scaling the synthesis of the final hybrid materials.

In this work, we report for the first time the successful intercalation of pure, non-functionalized C_{60} from organic solution into previously modified organophilic clays. C_{60} is a neutral molecule, insoluble in water, and hence cannot be introduced into the clay galleries by ion exchange or intercalation from water solution. To overcome this bottleneck, we organically modified the clay with quaternary amine by using well-established reactions in clay science prior to reaction with the C_{60} solution. The surfactant has two functions, namely to render the interlayer space organophilic and to expand the distance between the clay platelets. The expansion of the interlayer space allows the organic solvent (toluene) to enter into the clay galleries transferring along the fullerene molecules. Furthermore, we demonstrate the possibility to selectively remove the surfactant molecules either by simple ion-exchange reactions or by thermal treatment as to form novel pillared C_{60} clay structures. These novel C_{60}-pillared clays are very promising novel materials for gas storage and/or gas separation applications because they possess a high surface area (considerably higher than previously reported pillared clays).

Results and Discussion

In the first part of our study, the Na^+ exchangeable cations were replaced by a cationic surfactant to enhance the organophilicity of the parent clay and increase the interlayer spacing so that the organic solvent with the C_{60} could enter more easily. To prove that the interlayer spacing of the clay was indeed expanded by the introduction of organic cations and to demonstrate that the surfactant-exchanged clay can be intercalated with C_{60}, we employed X-ray diffraction to determine the d_{001} spacing. The powder XRD patterns of the surfactant-exchanged clay (sample denoted hereafter as Organo-SW_{y-1}) and of the fullerene-intercalated organoclay (sample denoted hereafter as C_{60}@Organo-SW_{y-1}) are shown in Figure 1.

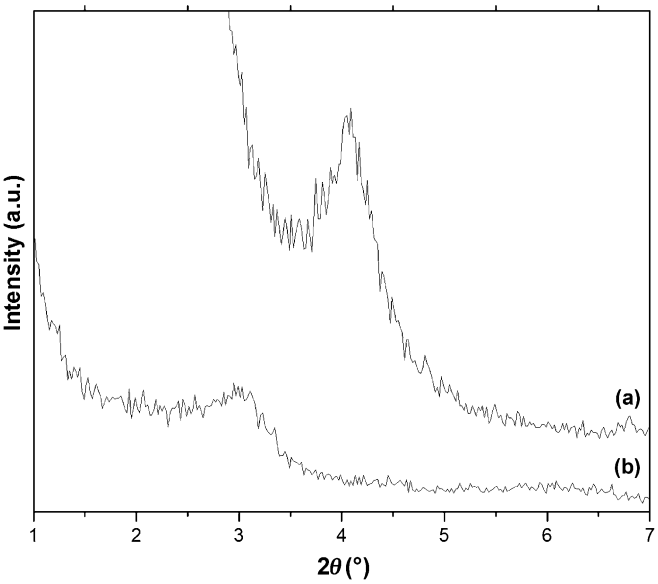

Figure 1. Powder X-ray diffraction patterns of a) Organo-SW_{y-1} and b) C_{60}@Organo-SW_{y-1}.

For Organo-SW_{y-1}, we found a d_{001} value of (21.5 ± 0.3) Å, which corresponds to a separation between clay platelets of $\Delta = 21.5–9.6$ Å $= 11.9$ Å, where 9.6 Å is the thickness of an individual clay platelet. This value implies that the flexible alkyl groups of the cationic surfactant adopt an inclined conformation when sandwiched between the clay surfaces. After the insertion of the fullerene, the Δ value of the re-

sulting C_{60}@Organo-SW_{y-1} was found to be 19.4 Å. This value is increased by 7.5 Å with respect to the corresponding value of Organo-SW_{y-1}. Noticeably, this value is very close to the size of the fullerene. As suggested by the recorded d_{001} values, the organic surfactant kept the interlayer space expanded and helped the toluene to penetrate, carrying along the neutral fullerene molecules. The latter stay embedded after evaporation of the organic solvent, being trapped by the previously intercalated surfactant molecules. A similar mechanism for the intercalation of chemically functionalized fullerene derivatives into the interlayer space of organoclays has been proposed in the past.[13] A schematic representation of the possible arrangement of the intercalated fullerene in Organo-SW_{y-1} is shown in Figure 3b assuming that the surfactant retains the conformation, which it acquired in the Organo-SW_{y-1} sample. According to the XRD results and the TEM results (see below) there is only one layer of fullerene entrapped in between the previously intercalated organic surfactant.

Another important information derived from the XRD pattern of C_{60}@Organo-SW_{y-1} was the absence of any reflection peaks of fullerite in the 2θ region 2–80°, indicating that molecules were not aggregated on the external clay surfaces after extensive washing of the product with toluene. This finding is further supported by the obtained TEM micrographs (see below). To further confirm the successful intercalation of C_{60} into the Organo-SW_{y-1}, the sample was annealed in order to selectively thermally remove the surfactant molecules. Diffraction patterns for various annealing temperatures are reported in Figure 2. When the C_{60}@Organo-SW_{y-1} sample was heated to temperatures above 150 °C, the characteristic 001 diffraction peak shifted to higher 2θ values, indicating a collapse of the interlayer space due to the removal of the surfactant molecules. However, the most interesting finding was the value of the interlayer distance recorded after prolonged heating (for 24 h) at 350 °C, a temperature where most of the surfactant molecules are thermally removed, but still considerably lower than the decomposition temperature of C_{60}. The recorded interlayer distance of approximately 7.4 Å coincides with the size of C_{60}. Moreover, both the position and the profile of the 001 diffraction peak remained the same even after cooling the sample to room temperature (Figure 2g), implying that the presence of C_{60} prevents the clay platelets from further collapsing. This proves that intercalation combined with heating results in a novel C_{60}-pillared clay structure (denoted hereafter as C_{60}@SW_{y-1}, Figure 3c).

To confirm the proposed model of C_{60} intercalation into the organoclay as well as the arrangement of the fullerene

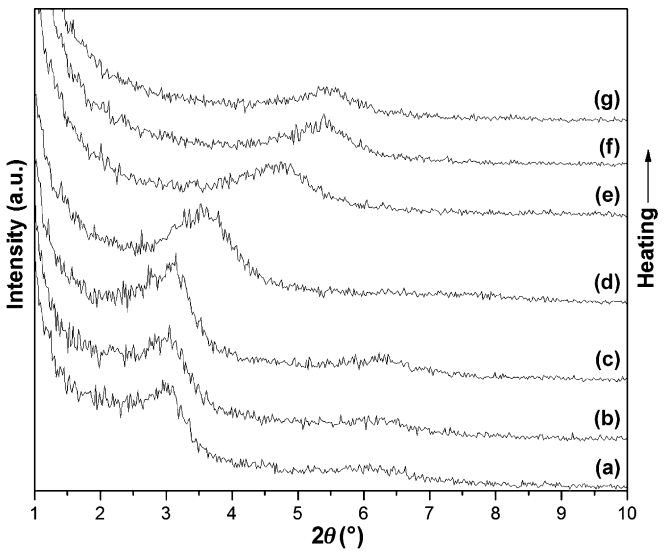

Figure 2. Powder X-ray diffraction patterns of C_{60}@Organo-SW_{y-1} measured after heating at a) 25, b) 100, c) 150, d) 250, e) 300, and f) 350 °C and g) after cooling down to 25 °C again.

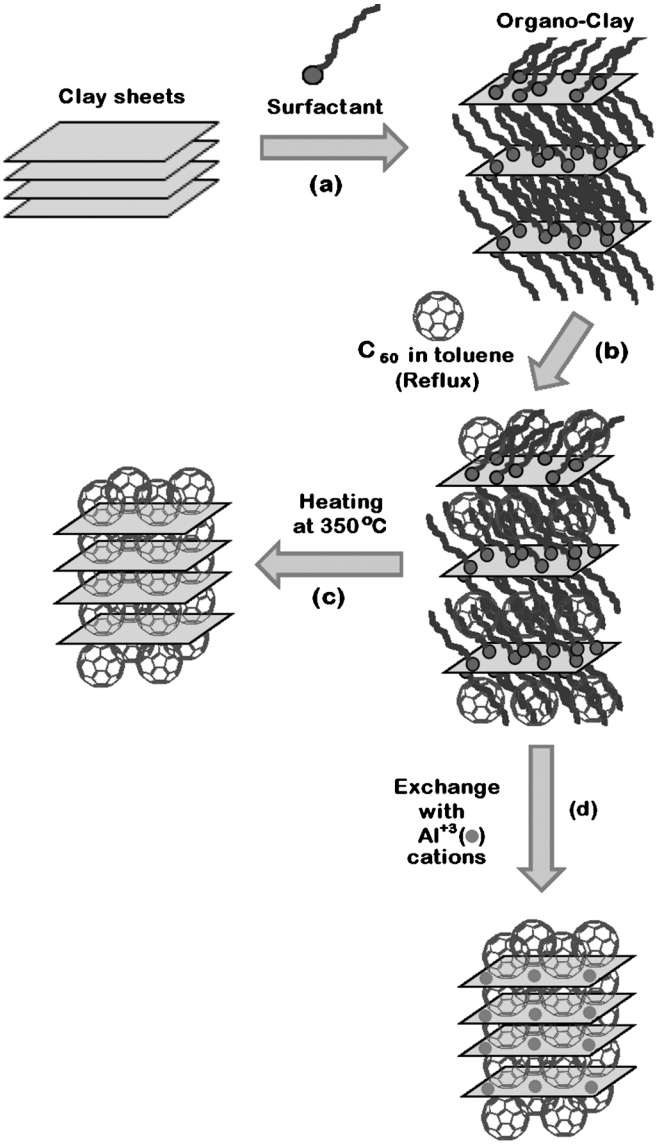

Figure 3. Schematic presentation of the organo-modification of a) the parent SW_{y-1} clay, b) the arrangement of fullerene in the organo-modified clay, c) the structures obtained after heating at 350 °C for 24 h, and d) after surfactant-exchange with Al^{3+} cations, before and after heating to 350 °C.

molecules within the interlayer space after the removal of the surfactant, High angle annular dark field scanning transmission electron microscopy (HAADF-STEM) analysis was performed on C_{60}@Organo-SW_{y-1}. In the HAADF-STEM images, the intensity is proportional to the Z number of the materials. Therefore, the clay shows white contrast due to its higher atomic numbers of the composing elements, whereas the intercalated organic moieties and fullerene appears to be darker due to light elements.

The images of the synthesized C_{60}@Organo-SW_{y-1} shown in Figure 4, clearly testify to the increment of the interlayer

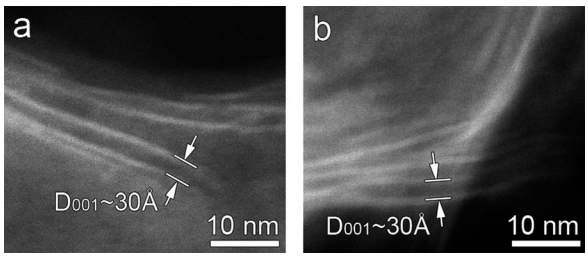

Figure 4. Characteristic STEM cross-sectional images of C_{60}@Organo-SW_{y-1}.

space (dark region) between the clay sheets (brighter regions) due to the incorporation of fullerene. The observed value of 30 Å is in agreement with the interlayer derived from the XRD measurements discussed above. On the contrary, the HAADF-STEM images collected on C_{60}@Organo-SW_{y-1} after prolonged heating at 350 °C (Figure 5) reveal a considerably reduced interlayer distance of about 15 Å, again in agreement with the XRD data discussed above. This confirms the selective removal of the organic molecules during the heat treatment and the formation of a C_{60}-pillared clay structure.

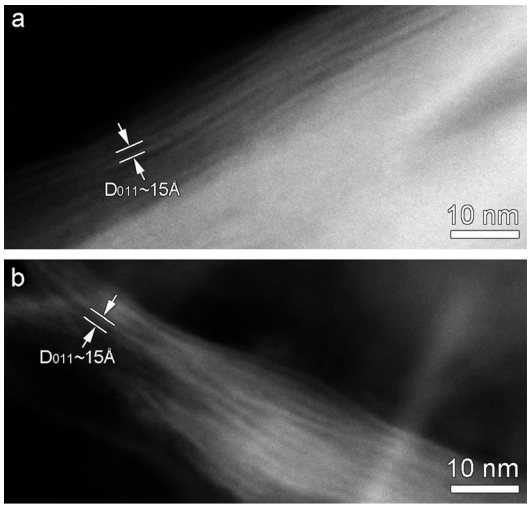

Figure 5. Characteristic STEM cross-sectional images of C_{60}@SW_{y-1} after prolonged heating at 350 °C.

We also explored the possibility to create a different kind of a C_{60}-pillared clay structure by exposing the C_{60}@Organo-SW_{y-1} sample overnight to a solution of $Al(NO_3)_3$, which should result in the selective removal of the organic surfactant from the interlayer space of the clay and its substitution by the inorganic cation (sample denoted hereafter as C_{60}@Al-exchanged-SW_{y-1}). By employing the diffraction pattern of C_{60}@Al-exchanged-SW_{y-1} (Figure S1b in the Supporting Information) the interlayer distance after the exchange reaction was found to be 7.3 Å. This value is significantly lower than that of C_{60}@Organo-SW_{y-1} and very close to the size of the buckminsterfullerene, suggesting that the surfactant molecules were successfully exchanged with the much smaller Al^{3+} cations. The size of the latter is smaller than C_{60} and hence the observed value of the d spacing is dictated by the size of the intercalated fullerene (Figure 3d).

The presence of fullerene in C_{60}@Organo-SW_{y-1} was further confirmed by UV/Vis spectroscopy. The UV spectrum of pure C_{60} dissolved in cyclohexane (Figure S2a in the Supporting Information) showed the characteristic sharp peaks at $\lambda = 257$ and 329 nm. The absorption spectrum of C_{60}@Organo-SW_{y-1} (Figure S2b in the Supporting Information) showed a similar profile but with the characteristic fullerene peak broadened and red shifted by 7 nm (to $\lambda =$ 264 nm) compared to the solution of pure fullerene. This result is in agreement with previous absorption studies in various media, where C_{60} or C_{60} derivatives are situated in the vicinity of polar interfaces.[13,16]

We also performed an elemental analysis by XPS to study the composition of the organoclay and of C_{60}@Organo-SW_{y-1}. In the case of Organo-SW_{y-1}, the characteristic Si 2p peak originating from the aluminosilicate framework[17] was recorded at a binding energy of 102.9 eV (Figure 6a, left). The C 1s photoemission line was found to comprise two components (Figure 6a, right); the major component, at a binding energy of 285.0 eV, is attributed to the C–C bonds of the methyl groups due to the intercalated surfactant molecules and accounts for 76% of the total carbon area, whereas the second peak at 286.6 eV originates mainly from the C–N bonds of the amine groups of the same surfactant molecules. The presence of the surfactant molecules was also evidenced by a single component at 402.9 eV in the N 1s spectrum (Figure 6b), which originates from the protonated amine end-tails of the surfactant.[18] In the case of C_{60}@Organo-SW_{y-1} the Si 2p peak is unchanged, whereas the C 1s photoemission line now requires four components in the deconvolution (Figure 7a, higher binding energy side). The first peak at 285.0 eV is assigned to the C–C bonds of the C_{60} cage and of the methyl groups of the surfactant molecules that are still present within the interlayer space as discussed above. The second peak at 286.6 eV is due to C–N bonds of the surfactant molecules. The two additional peaks at higher binding energies (288.6 and 291.0 eV) are attributed to the characteristic shake-up features of the C_{60}-cage.[19] The nitrogen spectrum of C_{60}@Organo-SWy-1 (not shown) did not reveal any significant differences compared to that of the organoclay.

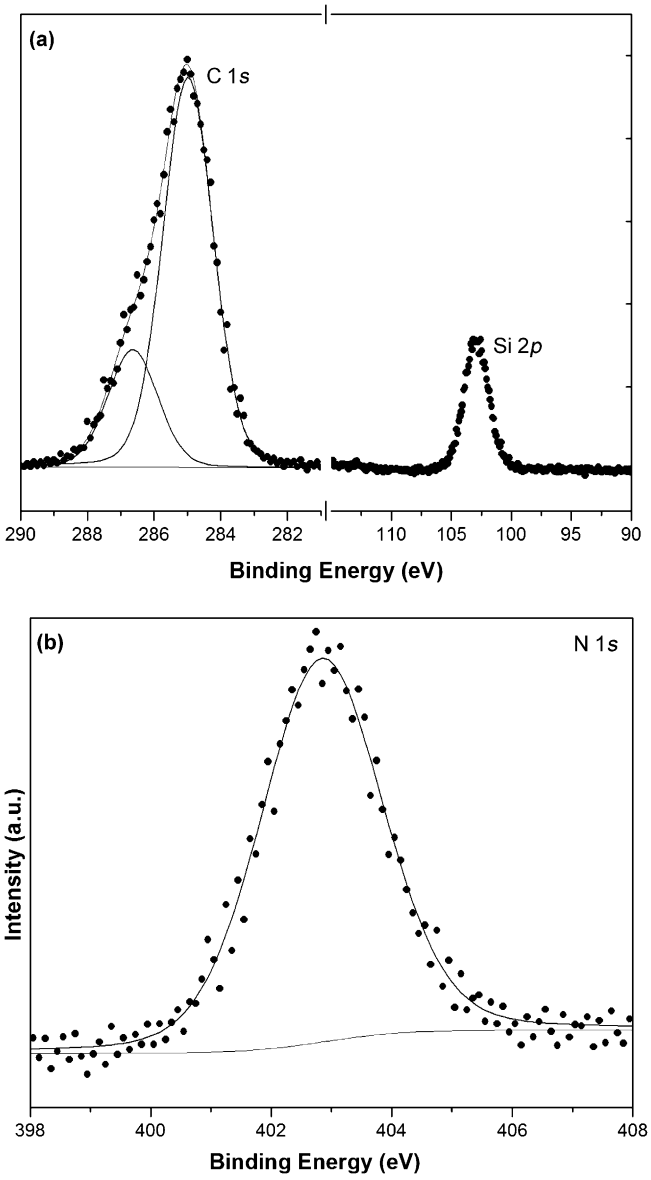

Figure 6. X-ray photoemission spectra of a) the C 1s and Si 2p and b) the N 1s core level regions of Organo-SW_{y-1} on Au/mica. Experimental data (●) and fit (——).

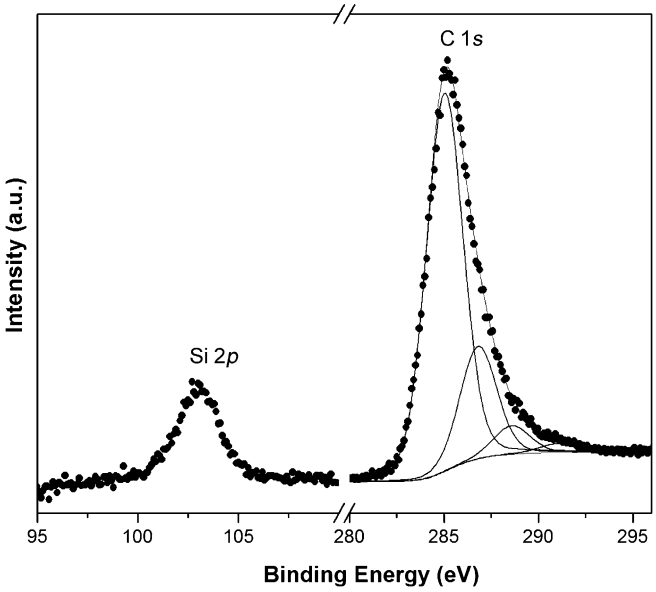

Figure 7. X-ray photoemission spectra of the C 1s and Si 2p core level regions of C_{60}@Organo-SW_{y-1} on Au/mica. Experimental data (●) and fit (——).

This implies that the intercalation of the C_{60} between the clay platelets did not change the chemical environment of the protonated amine end-groups of the surfactant, a suggestion that is in agreement with the XRD and TEM results discussed above, which suggested that C_{60} is sandwiched between the methyl end-groups of the intercalated surfactant and far away from the positively charged amine end-groups that interact with the negatively charged clay surfaces. XPS provides not only qualitative but also quantitative information[20] because the peak areas, normalized by the atomic sensitivity factors, are proportional to the amount of the corresponding atoms within the sampling depth. Within this context, the recorded relative ratio of the C 1s to the Si 2p peak areas of C_{60}@Organo-SW_{y-1} was found to be considerably higher (4.3) than the corresponding value of Organo-SW_{y-1} (2.6). This increase in the overall carbon content further confirms the incorporation of the C_{60} into the organoclay.

To further confirm the successful intercalation of the C_{60} and to probe the stability of the synthesized compounds, thermogravimetric analysis (TGA) of both Organo-SW_{y-1} and C_{60}@Organo-SW_{y-1} was performed in air. The TGA curve of Organo-SW_{y-1} (Figure S3a in the Supporting Information) showed an approximately 22% weight loss between 150 and 350°C, which is attributed to the thermal removal of the surfactant molecules from the clay galleries. Very similar weight loss of about 21% was recorded in the case of C_{60}@Organo-SW_{y-1} (Figure S3b in the Supporting Information). However, the thermal profiles of the two samples were totally different in the temperature region between 550 and 750°C where fullerene is expected to be thermally removed.[21] In detail, the weight loss of C_{60}@Organo-SW_{y-1} within this temperature range was found to be significantly higher (9%) than the corresponding one recorded for Organo-SW_{y-1} (4%), due to the presence of the fullerene in the hybrid material.

Nitrogen adsorption–desorption measurements (at 77 K) were performed on C_{60}-pillared clay, C_{60}@SW_{y-1}, obtained after heating C_{60}@Organo-SW_{y-1} to 350°C. The results are displayed in Figure 8. The observed shape of the hysteresis loop is typical for small, slit-shaped pores of layered materials resulting from the re-arrangement of the thin platelets of the fullerene-pillared montmorillonite after heating.[22] The surface area of the C_{60}@SW_{y-1} sample was calculated by using the Brunauer, Emmett, and Teller (BET)[23] equation and found to be 149 m^2g^{-1}. This value is considerably higher than the corresponding BET surface area value of the

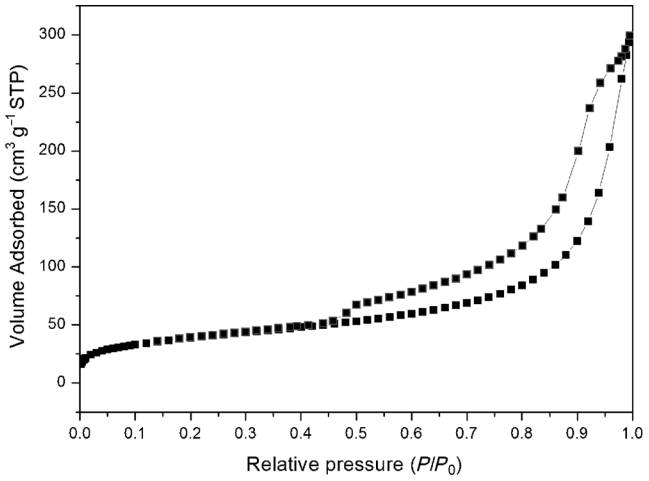

Figure 8. Nitrogen adsorption isotherms of C_{60}@ $Sw_{y-1.}$

parent montmorillonite clay, which is reported within the 20–40 $m^2 g^{-1}$ range,[24] confirming the successful pillaring from the incorporated fullerene molecules and revealing the great potential of the novel synthesized hybrids due to their increased surface area.

Conclusion

In conclusion, we report the successful incorporation of pure C_{60} from organic solution into clay. Because C_{60} is water insoluble, we organically modified the clay with quaternary amines prior to reaction with C_{60} solution in order to expand the galleries between the clay platelets and to modify their character from hydrophilic to organophilic. Furthermore, we demonstrated that the selective removal of the surfactant molecules either by simple ion-exchange reaction or by thermal treatment results in novel C_{60}-pillared clay. XRD, TEM, XPS, UV/Vis, and TGA measurements were employed to characterize the synthesized fullerene/clay hybrids and confirmed the successful intercalation of C_{60} into the interlayer space of the organoclay as well as the heating-induced pillaring process. The enhanced surface area deduced from porosimetry measurements of the C_{60}-pillared clay, together with its high thermal stability, inferred from TGA, are very promising for the use in gas storage and separation applications (e.g., as novel molecular sieve).

Experimental Section

Host layered material: The clay used was a natural Wyoming sodium montmorillonite (SW_{y-1}) obtained from the Source Clay Minerals Repository, University of Missouri (Columbia, MO), with a cation-exchange capacity (CEC) equal to 80 mequiv per 100 g clay. The clay was fractioned to <2 μm by gravity sedimentation and purified by well-established procedures in clay science. Sodium-exchanged samples (Na^+-SW_{y-1}) were prepared by immersing the clay into a 1 N solution of sodium chloride. Cation exchange was completed by washing and centrifuging four times with dilute aqueous NaCl solution. The samples were finally washed with deionized double-distilled water and transferred into dialysis tubes to obtain chloride-free clays and then dried at room temperature.

Preparation of organoclay: To prepare the organoclay, a solution of the surfactant (trimethyl hexadecylammonium chloride) in water ($3\times$CEC) was added to a stirred clay suspension of Na^+-SW_{y-1} (100 mg) in deionized double-distilled water (3 mL). The mixture was stirred, centrifuged, washed with deionized double-distilled water three times, and finally dried in air.[25]

Preparation of fullerene/organoclay: A purple-colored solution of C_{60} (15 mg) in toluene was mixed with a dispersion of organoclay (50 mg) in the same solvent (50 mL) and the mixture was heated to reflux at 110 °C for seven days. The solid was separated by centrifugation and washed several times with toluene in order to remove any unreacted fullerene residue that has crystallized on the external surfaces of the clay and finally dried in air.

Preparation of fullerene/Al-exchanged clay: A sample of the fullerene/organoclay (10 mg) was suspended in water (20 mL) and an excess of an aqueous $Al(NO_3)_3$ solution (1 M) was added. The mixture was stirred 48 h at ambient conditions, washed with deionized double-distilled water three times, and finally dried in air.

Powder X-ray diffraction (XRD): The XRD patterns were collected with a Philips PANanlytical X'Pert MRD diffractometer with a $Cu_{K\alpha}$ radiation ($\lambda=1.5418$ Å) by using an anode voltage of 40 kV and a current of 40 mA, a 0.25° divergent slit and a 0.125° anti-scattering slit. The patterns were recorded in a 2θ range from 1 to 10°, in steps of 0.01° with a counting time of 15 s each. Samples were in the form of films supported on SiO_x substrates. For the preparation of the films, aqueous suspensions of C_{60}/clay nanocomposites were deposited on the SiO_x plates, and the solvent was allowed to evaporate slowly at ambient temperature.

FTIR spectroscopy: Infrared spectra in the region $\tilde{\nu}=400$–4000 cm^{-1} were measured with a Bruker EQUINOX 55S infrared spectrometer, equipped with a deuterated triglycine sulfate (DTGS) detector. Each spectrum was the average of 200 scans collected at a resolution 2 cm^{-1}. Samples were in the form of KBr pellets containing approximately 2 wt% sample.

UV/Vis spectroscopy: Transmission UV/Vis spectra on dilute solutions of the samples in cyclohexane were obtained by a Shimadzu UV-1240 spectrophotometer.

X-ray photoemission spectroscopy (XPS): For the XPS measurements, evaporated gold films supported on mica were used as substrates. Pure clays or clay/fullerene nanocomposites were dispersed in deionized double-distilled (1 wt%) water, and after short stirring for 30 min, a small drop of the suspension was deposited on the Au substrate and left to dry in air. Samples were introduced through a load lock system into a SSX-100 (Surface Science Instruments) photoelectron spectrometer with a monochromatic $Al_{K\alpha}$ X-ray source ($h\nu=1486.6$ eV). The base pressure in the spectrometer was 1×10^{-10} Torr during all measurements. The energy resolution was set to 1.16 eV to minimize the measuring time. The photoelectron take-off angle was 37°. An electron flood gun providing 0.3 eV kinetic energy electrons in combination with an Au grid placed 1 mm above the sample was used to compensate for sample charging. All binding energies of the C_{60}/clay composites were referenced to the Si 2*s* core level of smectite clay at 102.8 eV.[26] Spectral analysis included a Shirley background subtraction[27] and peak deconvolution employing mixed Gaussian–Lorentzian functions, in a least squares curve-fitting program (WinSpec) developed at the LISE, University of Namur, Belgium.

Thermogravimetric (TGA) measurements: TGA measurements were recorded by using a Thermo Scientific thermogravimetric analyzer. Samples of approximately 10 mg were heated in air from 25 to 950 °C at a rate of 5 °C min^{-1}.

Transmission electron microscopy: High angle annular dark field scanning transmission electron microscopy (HAADF-STEM) was performed to investigate the interlayer distance of fullerene-intercalated clay. The HAADF-STEM was performed by using a FEI Titan 50-80 cubed microscope fitted with an aberration-corrector for the imaging lens and another for the probe forming lens as well as a monochromator. The HAADF-STEM investigation was operated at 120 kV in order to minimize possible beam damage to the intercalated structure including fullerene. The STEM convergence semi-angle was 21.4 mrad, providing a probe size of approximately 15 Å at 120 kV.

Specific surface area measurements: The nitrogen adsorption–desorption isotherms were measured at 77 K on a Sorptomatic 1990, Thermo Finnigan porosimeter. Specific surface areas (S_{BET}) were determined with the Brunauer–Emmett–Teller (BET) method[23] by using adsorption data points in the relative pressure P/P_o range of 0.01–0.25. The sample evaluated against surface analysis was out-gassed at 110 °C for 24 h under high vacuum (10^{-6} mbar) before acquiring the surface area measurements.

Acknowledgements

This work was carried out within the Top Research School Program of the Zernike Institute for Advanced Materials under the Bonus Incentive Scheme (BIS) of the Netherlands Ministry of Education, Science and Culture and received financial support from the Foundation for Fundamental Research on Matter (FOM), which is part of the Netherlands Organization for Scientific Research (NWO), and from the Breedtestrategie program of the University of Groningen. X. Ke and G. Van Tendeloo are grateful to the ERC grant "COUNTATOM".and the EC project ESMI.

[1] a) M. Prato, N. Martin, *J. Mater. Chem.* **2002**, *12*, 1; b) K. Prassides, *Physics and Chemistry of the Fullerenes*, Kluwer Academic, Dordrecht **1994**; c) K. M. Kadish, *Fullerenes: Chemistry, Physics and Technology*, Wiley, New York, **2000**.

[2] a) S. K. Pal, T. Kesti, M. Maiti, F. Zhang, O. Inganas, S. Hellstrom, M. R. Andersson, F. Oswald, F. Langa, T. Osterman, T. Pascher, A. Yartsev, V. Sundstrom, *J. Am. Chem. Soc.* **2010**, *132*, 12440–12451; b) A. Kraus, K. Mallen, *Macromolecules* **1999**, *32*, 4214–4219; c) S. Dai, P. Ravi, C. H. Tan, K. C. Tam, *Langmuir* **2004**, *20*, 8569–8575.

[3] a) C. D. Tran, V. I. Grishko, S. Challa, *J. Phys. Chem. B* **2008**, *112*, 14548–14559; b) F. Wudl, *J. Mater. Chem.* **2002**, *12*, 1959–1963; c) G. L. Closs, P. Gautam, D. Zhang, P. J. Krusic, S. A. Hill, E. Wasserman, *J. Phys. Chem.* **1992**, *96*, 5228–5231.

[4] a) W. Y. Tseng, J. T. Lin, C. Y. Mou, S. Cheng, S. B. Liu, P. P. Chu, H. W. Liu, *J. Am. Chem. Soc.* **1996**, *118*, 4411–4418; b) M. W. Anderson, J. Shi, D. A. Leigh, A. E. Moody, F. A. Wade, B. Hamilton, S. W. Carr, *J. Chem. Soc., Chem. Commun.* **1993**, 533–536.

[5] a) P. N. Keizer, J. R. Morton, K. F. Preston, A. K. Sugden, *J. Phys. Chem.* **1991**, *95*, 7117–7118; b) I. Piwonski, J. Zajac, D. J. Jones, J. Roziare, S. Partyka, S. Plaza, *Langmuir* **2000**, *16*, 9488–9492; c) C. H. Lee, T. S. Lin, H. P. Lin, Q. Zhao, S. B. Liu, C. Y. Mou, *Microporous Mesoporous Mater.* **2003**, *57*, 199–209.

[6] D. M. Guldi, F. Zerbetto, V. Georgakilas, M. Prato, *Acc. Chem. Res.* **2004**, *38*, 38–43.

[7] a) T. J. Pinnavaia, *Science* **1983**, *220*, 365–371; b) J. Konta, *Appl. Clay Sci.* **1995**, *10*, 275–335.

[8] J. A. Ballantine, *NATO-ASI Ser. Ser. C* **1986**, *165*, 197.

[9] a) V. Georgakilas, D. Gournis, A. B. Bourlinos, M. A. Karakassides, D. Petridis, *Chem. Eur. J.* **2003**, *9*, 3904–3908; b) V. Georgakilas, D. Gournis, D. Petridis, *Angew. Chem.* **2001**, *113*, 4416–4418; *Angew. Chem. Int. Ed.* **2001**, *40*, 4286–4288; c) T. Tsoufis, L. Jankovic, D. Gournis, P. N. Trikalitis, T. Bakas, *Mater. Sci. Eng. B* **2008**, *152*, 44–49.

[10] a) B. K. G. Theng, *The Chemistry of Clay Organic Reactions*, Adam Hilger, London, **1974**; b) T. Tsoufis, J. F. Colomer, E. MacCallini, L. Jankovič, P. Rudolf, D. Gournis, *Chem. Eur. J.* **2012**, *18*, 9305–9311.

[11] a) A. Gil, L. M. Gandia, M. A. Vicente, *Catal. Rev. Sci. Eng.* **2000**, *42*, 145–212; b) Y. Ma, W. Tong, H. Zhou, S. L. Suib, *Microporous Mesoporous Mater.* **2000**, *37*, 243–252; c) T. Shichi, K. Takagi, *J. Photochem. Photobiol. C* **2000**, *1*, 113–130.

[12] a) E. P. Giannelis, E. G. Rightor, T. J. Pinnavaia, *J. Am. Chem. Soc.* **1988**, *110*, 3880–3885; b) V. Lenoble, O. Bouras, V. Deluchat, B. Serpaud, J. C. Bollinger, *J. Colloid Interface Sci.* **2002**, *255*, 52–58; c) S. Moreno, R. Sun Kou, G. Poncelet, *J. Phys. Chem. B* **1997**, *101*, 1569–1578; d) M. Lim, Y. Zhou, B. Wood, L. Z. Wang, V. Rudolph, G. Q. Lu, *Environ. Sci. Technol.* **2008**, *43*, 538–543.

[13] D. Gournis, V. Georgakilas, M. A. Karakassides, T. Bakas, K. Kordatos, M. Prato, M. Fanti, F. Zerbetto, *J. Am. Chem. Soc.* **2004**, *126*, 8561–8568.

[14] D. Gournis, L. Jankovic, E. Maccallini, D. Benne, P. Rudolf, J. F. Colomer, C. Sooambar, V. Georgakilas, M. Prato, M. Fanti, F. Zerbetto, G. H. Sarova, D. M. Guldi, *J. Am. Chem. Soc.* **2006**, *128*, 6154–6163.

[15] a) M. Prato, M. Maggini, *Acc. Chem. Res.* **1998**, *31*, 519–526; b) F. Diederich, C. Thilgen, *Science* **1996**, *271*, 317–323.

[16] A. Lamrabte, J. M. Janot, A. Elmidaoui, P. Seta, L. C. de Ménorval, R. Backov, J. Rozière, J. L. Sauvajol, J. Allègre, *Chem. Phys. Lett.* **1998**, *295*, 257–265.

[17] L. M. Toma, R. Y. N. Gengler, E. B. Prinsen, D. Gournis, P. Rudolf, *Phys. Chem. Chem. Phys.* **2010**, *12*, 12188–12197.

[18] A. A. Tzialla, I. V. Pavlidis, M. P. Felicissimo, P. Rudolf, D. Gournis, H. Stamatis, *Bioresour. Technol.* **2010**, *101*, 1587–1594.

[19] D. Benne, E. Maccallini, P. Rudolf, C. Sooambar, M. Prato, *Carbon* **2006**, *44*, 2896–2903.

[20] D. Briggs, M. P. Seah, *Practical Surface Analysis*, Wiley, New York, **1990**.

[21] E. V. Basiuk, V. A. Basiuk, V. P. Shabel′nikov, V. G. Golovatyi, J. Ocotlán Flores, J. M. Saniger, *Carbon* **2003**, *41*, 2339–2346.

[22] a) S. Yamanaka, T. Nishihara, M. Hattori, Y. Suzuki, *Mater. Chem. Phys.* **1987**, *17*, 87–101; b) M. Pérez-Rea, F. Rojas, V. Castano, *Mater. Res. Innovations* **2003**, *7*, 341–352; c) Z. Ding, J. T. Kloprogge, R. L. Frost, G. Q. Lu, H. Y. Zhu, *J. Por. Mater.* **2001**, *8*, 273–293.

[23] S. Brunauer, P. H. Emmett, E. Teller, *J. Am. Chem. Soc.* **1938**, *60*, 309–319.

[24] a) J. Németh, I. Dékány, K. Süvegh, T. Marek, Z. Klencsár, A. Vértes, J. H. Fendler, *Langmuir* **2003**, *19*, 3762–3769; b) B. Lothenbach, G. Furrer, R. Schulin, *Environ. Sci. Technol.* **1997**, *31*, 1452–1462; c) P. Yuan, H. He, F. Bergaya, D. Wu, Q. Zhou, J. Zhu, *Microporous Mesoporous Mater.* **2006**, *88*, 8–15.

[25] A. A. Tzialla, E. Kalogeris, A. Enotiadis, A. A. Taha, D. Gournis, H. Stamatis, *Mater. Sci. Eng. B* **2009**, *165*, 173–177.

[26] E. Serefoglou, K. Litina, D. Gournis, E. Kalogeris, A. A. Tzialla, I. V. Pavlidis, H. Stamatis, E. Maccallini, M. Lubomska, P. Rudolf, *Chem. Mater.* **2008**, *20*, 4106–4115.

[27] D. A. Shirley, *Phys. Rev. B* **1972**, *5*, 4709.

Received: January 16, 2013
Published online: April 15, 2013

